ANSEICCA: a Python package for seismic ambient noise source inversion by cross-correlation modelling

Arjun Datta[a]

[a]*Department of Earth and Climate Science, Indian Institute of Science Education and Research, Pune, India*

ARTICLE INFO

Keywords:
Open-source
Python
Seismic ambient noise
Cross-correlation modelling
Waveform inversion
mpi4py
Devito

ABSTRACT

We present ANSEICCA, an open-source package for forward and inverse modelling of seismic ambient noise cross-correlations at local scales, where the effects of Earth's sphericity are negligible. The package implements a nonlinear finite-frequency inversion technique wherein measurements of cross-correlation energy are used to invert for the spatial distribution of ambient noise sources, under the assumption of a fixed Earth structure model. It is seamlessly integrated with other open-source Python packages for seismic wave propagation modelling, including a C-based numerical solver for acoustic modelling in 2-D media. It is a unique package insofar as the inversion is based on finite-frequency sensitivity kernels, but executed without the adjoint method. Instead, speed and computational efficiency are achieved by parallelising the code. Moreover, the Hessian-based optimization ensures convergence in a relatively small number of iterations (≈ 10), compared to purely gradient-based methods. We introduce the structure of the package in detail, describing both the serial and parallel versions of the code. Performance benchmarks show that ANSEICCA affords compute times of the order of a few minutes per iteration of inversion, with typical local-scale seismic array geometries.

This is a non peer reviewed pre-print submitted to EarthArxiv. It is being considered for publication in Computers and Geosciences.

1. Introduction

The ambient seismic field, or seismic ambient noise, is now one of the mainstays of seismological research. Interferometric techniques such as auto- and cross-correlation, are commonly used to extract meaningful signals from ambient noise recordings. Most applications exploit the assumption of Green's function retrieval from inter-station cross-correlations (Lobkis and Weaver, 2001; Shapiro and Campillo, 2004). In recent years, recognition of the limitations of this approach (e.g. Halliday and Curtis, 2008; Yao and van der Hilst, 2009; Kimman and Trampert, 2010; Fichtner, 2014) has prompted a parallel research track of interferometry using full-wave theory or 'interferometry without Green's function retrieval' (e.g. Fichtner et al., 2017; Fichtner and Tsai, 2019). In this unconventional approach, ambient noise cross-correlations are self-contained seismic observables which can be modelled through source and structure parameters, similar to traditional seismic observables from earthquake or explosive sources. This paper is concerned with using full-wave interferometry to invert for the spatial distribution of ambient noise sources.

Understanding the sources of ambient seismic signals is important for seismologists, because the source distribution

ORCID(s): 0000-0002-8249-9399 (A. Datta)

affects the accuracy of measurements that can be made by interferometry. A Green's function is recovered by cross-correlation only when the continuously recorded wavefield is diffuse, which in turn results either from strong multiple scattering, or from sources that are uniformly distributed or in the stationary phase region, with respect to the receiver pair (Snieder, 2004; Wapenaar, 2004; Wapenaar et al., 2010). This condition on the sources is often not satisfied in practice, and the seismological literature is replete with studies demonstrating the pitfalls of realistic ambient source distributions, in the context of Green's function retrieval (Pedersen and Krüger, 2007; Tsai, 2009; Yao and van der Hilst, 2009; Kimman and Trampert, 2010; Froment et al., 2010; Tsai, 2011; Wang et al., 2016; Stehly and Boué, 2017). A number of seismological studies primarily aimed at imaging Earth structure, have tried to explicitly account for ambient noise source distribution (Roux, 2009; Delaney et al., 2017; Lehujeur et al., 2017). Yet others have been devoted exclusively to studying the sources themselves (Ermert et al., 2016, 2017; Sager et al., 2018a; Igel et al., 2021, 2023; Xu et al., 2019). More widely in the geosciences, these ambient seismic sources shed light on a wide range of natural phenomena. These include, but are not limited to, ocean wave coupling with the seafloor (e.g. Juretzek and Hadziioannou, 2016), sediment transport in rivers (Tsai et al., 2012), glacier hydrology and dynamics (e.g. Aso et al., 2017; Labedz et al., 2022), tropical cyclones (e.g. Retailleau and Gualtieri, 2019) and underground hydrothermal activity (e.g. Cros et al., 2011).

Very few open-source codes for full-wave interferometry are available, perhaps reflecting its inherent mathematical and computational complexity compared to the conventional approach of Green's function retrieval. SPECFEM3D (Tromp et al., 2010) contains an implementation of noise cross-correlations and sensitivity kernels, but is cumbersome to use for inversion, as noted by Ermert et al. (2020). With specific regard to noise source inversion, where a fixed Earth structure model (of density and seismic velocities) is assumed, the only dedicated open-source code we are aware of, is the Python package called `noisi` (Ermert et al., 2020). `noisi` was developed for regional to global scale applications (e.g. Igel et al., 2021). Here we present ANSEICCA, an ambient noise source inversion package, also in Python, but tailor made for local-scale applications. Ambient noise studies at the local scale can be used for tomography, but are also important for other applications such as the analysis of site effects (e.g. Roten et al., 2006; Denolle et al., 2013; Bowden et al., 2015). Due to the relatively lower demands of local-scale seismic modelling, ANSEICCA espouses a different computational philosophy than `noisi`. Rather than utilizing pre-computed databases of Green's functions to model seismic wave propagation from ambient noise sources, it generates these on the fly. Additionally, there are technical differences pertaining to the particular form of forward and inverse modelling used, as also the manner in which inversion is implemented.

ANSEICCA can be a useful tool for seismologists interested in the rigorous modelling and inversion of ambient noise cross-correlations. It may be particularly helpful to new researchers or those from other fields who wish to venture into the realm of full-wave seismic interferometry, but are deterred by the dense mathematical formulation of adjoint methods. ANSEICCA harnesses the power of full-wave theory and finite frequency sensitivity kernels, without using adjoint techniques to compute the kernels (see Datta et al., 2023). Source sensitivity kernels are computed for each individual pair of receivers. This sacrifices computational efficiency (the compute time increases non-linearly with the number of receivers), but access to individual kernels offers the advantage that one can calculate the Hessian for the inverse problem, not just the gradient.

To alleviate the issue of compute time scaling with the number of receivers, we parallelise the code using *mpi4py* (Dalcín et al., 2005). The parallelised implementation makes ANSEICCA efficient and practically useful for realistic applications. Finally, we note that whilst ANSEICCA is primarily intended to be an inversion tool, it can, like `noisi`, also be used simply for cross-correlation modelling (e.g. Malkoti et al., 2021). This is useful to study the influence of noise sources on ground motion auto-correlations, or on specific measurements such as attenuation (e.g. Stehly and Boué, 2017) or Rayleigh wave ellipticity (Malkoti et al., 2021). Moreover, it can be used to assess the quality of empirical Green's functions retrieved from ambient noise cross-correlations (for various source scenarios and heterogeneous Earth models), as an alternative to brute-force numerical experiments (Wapenaar et al., 2010; Fichtner, 2014; Tkalčić et al., 2020).

The first version of ANSEICCA (Datta et al., 2019) had limited applicability as it could only handle a homogeneous acoustic medium. Since then the code has been refined as well as advanced, to incorporate increasing levels of forward modelling rigour, culminating in the recent work by Datta et al. (2023), who incorporated 2-D acoustic modelling. The current version of ANSEICCA, presented in this paper, incorporates three different forward modelling regimes, all in one code package. Although the theoretical foundations of each technique advancement have been documented in past papers, this paper focuses on the code and provides a comprehensive overview. We first present the modelling methods and their implementation (Section 2), then describe the code in detail (Section 3), and finally provide some performance benchmarks (Section 4).

2. Modelling methods

This is an inversion package for estimating seismic ambient noise source distributions. It requires a forward model for interstation cross-correlations arising from distributed noise sources, and inversion is performed using sensitivity kernels for cross-correlation amplitudes/energy. Both the forward and inverse modelling schemes are described in this section, with a focus on computation and code implementation.

2.1. Forward modelling

Given a spatial distribution, $\sigma(\mathbf{x})$, of ambient noise sources with power spectrum $P(\omega)$, the cross-correlation $C(\mathbf{x}_A, \mathbf{x}_B)$ of ambient noise recorded at receiver locations $\mathbf{x}_\mathrm{A}$ and $\mathbf{x}_\mathrm{B}$ is modelled in the frequency domain using the medium Green's function G, as:

$$C(\mathbf{x}_A, \mathbf{x}_B; \omega) = P(\omega) \int d^2\mathbf{x}\; G^*(\mathbf{x}_A, \mathbf{x}; \omega) G(\mathbf{x}_B, \mathbf{x}; \omega) \sigma(\mathbf{x}), \tag{1}$$

in the scalar/acoustic scenario (Datta et al., 2019, 2023), and as

$$C_{pq}(\mathbf{x}_A, \mathbf{x}_B; \omega) = P(\omega) \int d^2\mathbf{x}\; G^*_{pi}(\mathbf{x}_A, \mathbf{x}; \omega) G_{qi}(\mathbf{x}_B, \mathbf{x}; \omega) \sigma(\mathbf{x}), \tag{2}$$

in the elastic scenario (Malkoti et al., 2021; Datta, 2023). In both the above equations, the asterisk denotes complex conjugation. The Green's function as well as cross-correlation are scalar quantities in Equation (1), but tensors in Equation (2), where subscripts p and q denote the components of motion at receivers $\mathbf{x}_A$ and $\mathbf{x}_B$ respectively, while subscript i refers to the direction of impulsive force at the source location $\mathbf{x}$.

The forward model represented by equations (1) and (2) corresponds to ensemble-averaging of spatially uncorrelated noise sources (e.g. Tromp et al., 2010; Fichtner et al., 2017; Fichtner and Tsai, 2019), subject to the following additional assumptions:

(i) The power-spectral density of the noise sources, $S(\mathbf{x}, \omega)$, is separable into position-dependent, and frequency-dependent terms, i.e. $S(\mathbf{x}, \omega) = P(\omega)\sigma(\mathbf{x})$. In other words, noise sources everywhere have the same spectral shape $P(\omega)$, only their strength is modulated by the function $\sigma(\mathbf{x})$.

(ii) In the elastic case, it is assumed that all noise sources are point forces acting in the same direction, so that S is still a scalar quantity and we do not have to consider the tensor S_{ij}.

We acknowledge that the first assumption listed above, limits the code versatility. It cannot be blindly applied to scenarios where ambient seismic sources with very different frequency spectra (e.g. anthropogenic sources and ocean microseisms) may be active in comparable measure. In order to use the package in such scenarios, it will be prudent to perform source inversion in different frequency bands, each with its own $P(\omega)$.

An efficient way to evaluate the integrals in equations (1) or (2), is to invoke source-receiver reciprocity, turning both receiver locations into sources (Hanasoge, 2014; Xu et al., 2019). This is the approach taken in the ANSEICCA package, as detailed below. It is generally applicable because of assumption (i) listed above, which puts $P(\omega)$ outside the integral. Without this convenience, we note that Equation (3) below is not valid, and alternative computational techniques, such as the 'three-step' approach (see e.g. Tromp et al., 2010; Sager et al., 2018b), need to be employed.

2.1.1. Implementation

ANSEICCA is purely a source inversion package and it works by assuming a fixed Earth structure model. Currently it is compatible with homogeneous acoustic, 1-D (depth dependent) elastic, and 2-D (laterally varying) acoustic media. Although 3-D elastic modelling is not yet incorporated, we note that some features of surface wave propagation are in fact captured by acoustic modelling. It is well known that the acoustic wave equation describes the motion of an elastic membrane, and that the scalar, 2-D Green's function of membrane waves is formally related to the surface wave Green's function (Tromp and Dahlen, 1993).

The precise evaluation of equation (1) or (2) depends on the type of medium assumed:

1. Homogeneous acoustic medium – in this case the Green's function takes the analytic form $G(\mathbf{x}_A, \mathbf{x}; \omega) = H_0^{(1)}\left(\frac{\omega}{c}|\mathbf{x}_A - \mathbf{x}|\right)$, where $H_0^{(1)}$ is the Hankel function of the first kind of zeroth order, and c is the scalar wavespeed. This type of Green's function is internally calculated within the package (Datta et al., 2019).
2. 1-D elastic medium – here we use the surface wave terms of the elastodynamic Green's function, which are semi-analytically computable using surface wave theory in 1-D media (Malkoti et al., 2021; Datta, 2023). This type of Green's function is calculated by importing an external module from the package *SW1D_earthsr*, which is a separate package available from AD's Github repository. This package is tied to the surface wave code 'earthsr' (see Datta et al., 2017; Datta, 2018), which is based on the propagator matrix technique of Gomberg and Masters (1988).
3. 2-D acoustic medium – in this case we re-write equation (1) as

$$C(\mathbf{x}_A, \mathbf{x}_B) = \int d^2\mathbf{x}\; u^*(\mathbf{x}_A, \mathbf{x})\; u(\mathbf{x}_B, \mathbf{x})\; \sigma(\mathbf{x}), \tag{3}$$

with $u(\mathbf{x}_A, \mathbf{x}) = P(\omega)^{1/2} G(\mathbf{x}_A, \mathbf{x})$. Note that we have dropped the dependence on angular frequency ω, in the interest of a condensed notation. The wavefields u in equation (3) are obtained by numerically solving the acoustic wave equation with a source term equal to $P(\omega)^{1/2}$. This step of computing the wavefields is outsourced to the open-source Python package *Devito*, which implements finite difference modelling of seismic wave propagation (Louboutin et al., 2019; Luporini et al., 2020). Source-receiver reciprocity is invoked just as is done for equations (1) and (2), implying that N numerical simulations are required in total, one per source at each of the N receivers (Datta et al., 2023).

In all three scenarios, once the appropriate Green's functions or wavefields are available, the cross-correlation for any pair of receivers is computed by approximating the spatial integrals of equations (1)-(3), as weighted sums over the modelling domain, similar to `noisi`. For example, equation 1 is implemented as:

$$C(\mathbf{x}_A, \mathbf{x}_B; \omega) \approx P(\omega) \sum_s \left[G^*(\mathbf{x}_s, \mathbf{x}_A; \omega) G(\mathbf{x}_s, \mathbf{x}_B; \omega) \sigma(\mathbf{x}_s) \right] (\Delta \mathbf{x})^2, \tag{4}$$

where the subscript s denotes individual grid points. This subscript is dropped from $\Delta\mathbf{x}$ because the grid is uniform. The errors introduced by the approximation represented in equation (4), have been analysed in detail by Ermert et al. (2020).

In this way, the ANSEICCA package separates the forward modelling into two steps — 'primary forward modelling', i.e. computation of Green's functions or wavefields, and the multiplication-summation required to evaluate the cross-correlation integral. This is in contrast to the aforementioned three-step approach, which does away with the need for multiplication and summation, but requires $2N$ numerical simulations (two simulations per receiver) in every iteration.

We note that ANSEICCA has been integrated with specifically chosen external packages, for the purpose of primary forward modelling in heterogeneous media. These packages may be replaced by others in the future, with minimal changes to the ANSEICCA code. All that is required is an interface module that takes the necessary parameters from ANSEICCA, and provides it the necessary Green's functions or wavefields. In this context, we also note that our package is currently not compatible with pre-computed databases of Green's functions or wavefields (e.g. *noisi* by Ermert et al., 2020). While this too can be implemented, we do not believe this will provide a major benefit because primary forward modelling is not a bottleneck of our code, for the reason discussed below.

2.1.2. Code optimization

In order to optimize the implementation described above, it is important to first note that primary forward modelling needs to be performed only once (it is done before the start of the iterative inversion – see Figure 4, Section 3), because the structure model is held fixed and hence G or u, do not change through the iterations. On the other hand, the cross-correlation integral needs to be evaluated afresh every iteration, because $\sigma(\mathbf{x})$ changes as the inversion proceeds. Hence from the point of view of optimization, it is important to focus on the integral evaluation. Equations (1)-(3) need to be applied to all pairs of receivers, which implies ${}^N C_2$ multiplication-summation operations, i.e. $O(N^2)$ operations, every iteration. This loop over receivers is a time-consuming exercise, which can be sped up by parallelization (see Section 3.3).

While the optimization of the primary modelling is less important, we have not ignored it.

1. Homogeneous and 1-D media: both these types of media are laterally homogeneous. We exploit the translational invariance of wave solutions in a laterally homogeneous medium, by primary forward modelling for a single source, rather than N sources. By choosing an 'outer domain' which is twice the size (four times the area) of the

actual (square) modelling domain, it is possible to simulate the wavefield due to a source at any location within the actual domain. This is illustrated in Figure 1. In this way, the Green's function due to a source at each of the N receivers, is obtained by modelling the solution due to a single source at the centre of a larger domain.

2. 2-D media: in this case, wavefields are computed using *Devito*, which generates highly optimized low-level C code for finite-difference solution of the acoustic wave equation.

2.2. Inversion

The aim of the inversion is to retrieve the source distribution $\sigma(\mathbf{x})$, using observations of cross-correlations $C(\mathbf{x}_A, \mathbf{x}_B)$ for numerous receiver pairs $(\mathbf{x}_A, \mathbf{x}_B)$ within a receiver network. Unlike the forward theory described in Section 2.1, which is implemented with various modelling options, inverse modelling within the ANSEICCA package is rigidly implemented. It is predicated on matching the energies of observed and predicted cross-correlation waveforms. The misfit functional used to compare observed and predicted cross-correlations is (Hanasoge, 2013):

$$\chi = \frac{1}{2} \sum_i \left(\ln \frac{E_i^{\text{obs}}}{E_i^{\text{syn}}} \right)^2 , \tag{5}$$

where the index i runs over all receiver pairs and E is the waveform energy in a time window $w(t)$:

$$E_{AB} = \sqrt{\int w(t) C_{AB}^2(t)\, dt}, \tag{6}$$

C_{AB} being shorthand for $C(\mathbf{x}_A, \mathbf{x}_B)$. Inversion is driven by the so-called 'source kernels', which describe the sensitivity of cross-correlation energy to the source distribution $\sigma(\mathbf{x})$:

$$K_{AB}(\mathbf{x}) = \int d\omega\, f(\mathbf{x}_A, \mathbf{x}_B; \omega)\, G^*(\mathbf{x}_A, \mathbf{x}; \omega)\, G(\mathbf{x}_B, \mathbf{x}; \omega) P(\omega) \tag{7}$$

$$\text{OR} \int d\omega\, f(\mathbf{x}_A, \mathbf{x}_B; \omega)\, u^*(\mathbf{x}_A, \mathbf{x}; \omega)\, u(\mathbf{x}_B, \mathbf{x}; \omega). \tag{8}$$

The function f in equations (7)-(8) depends on the particular misfit used. Given the logarithmic misfit (5), Hanasoge (2013) obtained:

$$f(\mathbf{x}_A, \mathbf{x}_B; \omega) = \left(\frac{1}{E_{AB}^{syn}} \right)^2 C_{AB}^*(\omega) \tag{9}$$

The finite frequency kernels $K_{AB}(\mathbf{x})$ are continuous functions, but they are applied to a discrete inverse problem by parameterizing the model space in terms of a finite set of basis functions (see equation (12) in the Appendix). The inverse problem therefore reduces to a problem of estimating the basis function coefficients, which can be solved by any of the standard optimization techniques of discrete inverse theory. We use the Gauss-Newton method, as detailed in Section (Appendix) 8. Note that optimization is not directly applied to the quantity of interest, $\sigma(\mathbf{x})$, but to the basis function coefficients, m_j. The former must be obtained from the latter using equation (12).

2.2.1. Implementation

The ANSEICCA package contains a raw implementation of the inversion scheme detailed in Section (Appendix) 8. Similar to forward modelling, the inversion process can be seen as separated into two parts — calculation of measurements and kernels, which is done within the package's core module (*h13*, see Table 1), and optimization using the Gauss-Newton algorithm, which is handled by one of the utility modules (*u1*, see Table 1). The code is structured such that both parts are integrated into an explicit *while* loop, which runs until the inversion converges or hits a cap on the number of iterations. This structure is facilitated by the fact that the optimization does not rely on any in-built Python routines, such as from the SciPy minimize module[1]. Instead, after computing the gradient and approximate Hessian in any iteration, equation (20) is explicitly solved (using NumPy's *linalg* module) to obtain the model update. The entire inverse modelling workflow, from measurements to optimization, is implemented separately for positive and negative-branch measurements, and the results averaged at the end of an iteration, to update the model.

Inversion is deemed to have converged when the data misfit ceases to change (decrease) by more than a threshold value (e.g. 2 or 5%), which is hardwired into the code. Synthetic tests reveal that this typically happens in a relatively small number of iterations, on the order of 10. Figure 2 shows the progress of inversion in the 'E1' example provided with the package.

2.2.2. Code optimization

The bottleneck in the inversion workflow described above, is the calculation of pairwise source kernels. This calculation is parallelized in the same way as the evaluation of cross-correlation integrals for forward modelling (see Section 3.3).

3. Detailed code description

The source code of the ANSEICCA package comprises two directories: *anseicca* and *modules_common*. Two types of code are contained within *anseicca*: serial and parallel. Each comes with its own 'wrapper' program (*anseicca_wrapper_serial* or *anseicca_wrapper_parallel*) and core module (*hans2013_serial* or *hans2013_parallel*), but all other modules are common to the serial and parallel codes. These modules are also shared with a related but separate package of code, currently under development, which is meant for structure inversion. Hence these modules are bundled together in the appropriately-named *modules_common* directory.

[1] we have tried the L-BFGS and conjugate-gradient algorithms from `scipy.minimize`. Use of this module requires non-trivial modification of the code (no explicit loop over iterations) and does not produce improved results, therefore we have not retained this option in the code.

Module	Shorthand
In *anseicca*:	
hans2013_serial.py or *hans2013_parallel.py*	h13
In *modules_common*:	
cctomo_utis1.py	u1
cctomo_utis2.py	u2
utis_io.py	uio
validate_params.py	val

Table 1
Code modules and corresponding short names used in this paper.

Figure 3 shows the overall code structure. It represents a sequential workflow that is fully automated by the wrapper programs. Therefore, from a user perspective, performing an ambient noise source inversion is simply a matter of running the code wrapper, once all necessary inputs are in place (see section 3.2.1). However, it is emphasized that this code package inverts ambient noise cross-correlograms, not raw seismic ambient noise recordings. To perform noise source inversion with this package, one first needs to generate cross-correlation data (by external means) from raw noise data. It is assumed that the processing applied to the raw data to obtain cross-correlograms (e.g. Bensen et al., 2007) includes bandpass filtering, so that the data input to the package has a well-defined bandwidth. This bandwidth helps define the $P(\omega)$ used for forward modelling (see section 3.4).

3.1. Running the code

To run the serial or parallel code, one runs the corresponding wrapper program (specifying the correct number of processors in the parallel case, see Section 3.3). Two controls are provided in the wrappers, via the following boolean flags:

1. *do_inv*: if *True*, the code executes to completion – as determined by the second flag described below – and produces an output file (see Section 3.2.2). If set to *False*, the code executes only up to the 'set up' stage; no forward or inverse modelling is performed, and no output file produced. The *False* setting is useful for plotting and visualization purposes.
2. *iter_only1*: if *False*, inversion proceeds until 'natural' termination as per the criteria laid out in Section 2.2. If set to *True*, the inversion is force-terminated after one iteration. The *True* setting is useful for testing and forward modelling purposes.

All other code settings, including parameter specifications, are provided in a parameter file called *Par_file*, which is described in detail in the code manual. Beginners or novice programmers need only interface with the wrapper and the *Par_file*, to use the code as is.

3.2. I/O

The primary input to the code is the cross-correlation data to be inverted, and the primary output is the spatial source distribution obtained by inversion. Additional I/O essentially constitutes supporting information. From a seismic data processing perspective, it must be emphasized that this package does not compute ambient noise cross-correlagrams from raw seismic data. The correlograms must be generated externally, and provided as an input to the package. All of the code's I/O operations are handled by the *utils_io* module.

3.2.1. Input

The fundamental input to the package is three-fold: two files, with hardwired names and locations, and one data directory:

(i) *receivers.csv*: a text file containing the list of stations or receivers with their IDs and location coordinates (see manual for format). Needs to be present in the *INPUT* sub-directory within *anseicca*.

(ii) *Par_file*: a text file specifying the values of various simulation parameters (see manual for detailed description). This file must be compatible with *modules_common/config.py*, which reads it using Python's *configparser* utility. Needs to be present in the *INPUT* sub-directory within *anseicca*.

(iii) Data: a single directory containing observed interstation cross-correlations. Compatible data formats are detailed in the code manual. Note that the code can handle 'missing data', so the cross-correlations available in the data directory, may correspond to any subset of all possible station pairs. The recommended location for this directory is *anseicca/INPUT/DATA*.

In addition to these core inputs, the code may require other inputs depending on the use case. These auxiliary inputs are obtained interactively via user prompts (generated in accordance with the relevant*Par_file* settings):

(a) 1-D elastic model(s): a single directory containing an elastic Earth model file, plus the associated dispersion and eigenfunction files compatible with the *SW1D_earthsr* package (Section 2.1.1?). This input is required when analytical, elastic modelling is chosen for inversion and/or for the generation of test data (in *Par_file* settings).

(b) 2-D velocity model(s): a single file to be used either for inversion, or for the generation of test data (two separate files may be provided for the two purposes). This input is required when numerical, acoustic modelling is chosen for inversion and/or test data generation (in *Par_file* settings). The velocity model files must be in *.npz* format, compatible with *modules_common/read_velocity_models.py*.

(c) Receiver list: a single file specifying the receiver IDs to be included in the simulation, with a single receiver per line. This input is solicited (not required) whenever the number of receivers in the *Par_file* is set to less than the total number of receivers contained in *receivers.csv*. If no input is provided, the desired number of receivers is selected automatically using an internal criterion (which penalises receiver location error arising from mapping specified receiver coordinates, onto a uniform grid).

With reference to the data input to the package, we note that it can be omitted when running synthetic tests (e.g. Datta et al., 2023). In this case the 'data' need not be pre-existing and stored on disk. As a legacy from its humble origins in the MATLAB code of Hanasoge (2013), the anseicca package is designed to include an 'internal data' mode (*Par_file* setting: *ext_data = False*), in which synthetic data is generated internally for a chosen 'true model', stored in memory, and then inverted — all in a single code run. In order to avoid the 'inverse crime' of computing and inverting 'data' using the same modelling scheme, one only needs to specify different modelling parameters for the generation of test data, and for inversion. The *Par_file* and the auxiliary input are designed to specify these two sets of parameters completely independently. For example, Datta et al. (2019) had demonstrated the use of different model parameterizations for the test data and inversion. Datta et al. (2023) additionally showed how, with acoustic modelling, different velocity models can be used in the two cases.

We use the terms 'internal data' and 'external data' for data generated internally, and data read from disk, respectively. Internal data is always synthetic, whereas external data may be real or synthetic.

3.2.2. Output

The output of the code, regardless of whether serial or parallel, consists of a single *.pckl* file produced using Python's *pickle* module. In addition to the results (both final and intermediate) of a code run, the output file contains all the necessary settings and parameter values required to reproduce the run. This can save users a lot of tedious bookkeeping, as simulation parameters do not need to be recorded or documented separately.

The *view_output_anseicca.py* script, in the *anseicca* directory, can be used to visualize the output. It relies on *read_pickled_output.py*, from *modules_common*, to de-serialize the input, and provides a host of options for plotting various quantities. The code manual provides a comprehensive demonstration of all plotting options, several of which have been used to produce figures shown in this paper as well as previous related ones.

Finally, *view_output_anseicca.py* also allows the user to save the (synthetic) cross-correlation waveforms generated during a code run and contained in the output file, as individual SAC files. This can be used to create a directory of 'data', which can serve as input to the code in a future run.

3.3. Parallelization

As depicted in Figure 3, only the core module of this package, *h13*, is parallelized. All other processes in the overall code flow, are executed exclusively on the master processor (rank = 0). Within the core module, the computationally expensive processes are cross-correlation modelling, and the calculation of pairwise source kernels (see Figure 4). Both of these require multiplication and summation operations to be performed for every pair of receivers. This implies

$O(N^2)$ calculations, for N receivers. In the serial code, these processes are each implemented via a nested for-loop structure. On the other hand, the parallel code distributes the pairwise calculations across processors, reducing the number of operations from $O(N^2)$ to $O(N)$, per processor. Therefore the speed-up achieved by parallelization, scales with N.

It works by setting the number of processors to be equal to the number of receivers. The i^{th} processor is assigned the task of performing the calculations for all receiver pairs (j, i), where $i < j \leq N$. Thus the i^{th} processor handles $N - i$ receiver pairs, implying that the first processor performs the most calculations, and the last processor performs none.

In the calculation of source kernels, we note that results from individual processors need to be combined to build the complete **G** (Jacobian) matrix, because each processor can contribute only some part (rows) of this matrix, through equation (16).

Finally, we wish to point out that the parallelization described here refers only to code operations performed within the ANSEICCA package. In the rigorous use case of 2-D acoustic modelling, the primary forward modelling (outsourced to Devito) may itself be computationally demanding, but is currently not parallelized. However this is not a major bottleneck because of reasons noted earlier:

(a) the number of numerical simulations required is N, not $O(N^2)$

(b) these simulations need to be performed only once, not repeated every iteration.

3.4. Working with real data

Inversion of real data involves a few important considerations and code operations, which are exclusive to the external data usage mode. These details are hidden in the flowcharts of Figures 3 and 4, so we highlight them in this section. The u2 module has been devoted to these specific operations, as detailed below:

1. Estimation of signal-to-noise ratio (SNR) – this is part of the 'read and process data' step in Figure 3. The u2 module's *cc_data* class, which reads the data, includes a *Process* sub-class which calculates the SNR of the individual cross-correlation waveforms. The SNR values are converted to data errors, which constitute the data covariance matrix used in inversion (see Section 2.2). Conversion of SNR to error values is subject to user discretion (e.g. Datta et al., 2019), but must be hardwired into the u2 module.
2. Choice of measurement window – the time window $w(t)$ used to define the data measurement is taken to be the same as that used to calculate SNR valules. Hence the choice of $w(t)$ is also hardwired into the u2 module.
3. Estimation of $P(\omega)$ – this is done in two stages. First, as part of the 'read and process data' step in Figure 3, the shape of $P(\omega)$ is determined by averaging the power spectra of all the cross-correlation waveforms in the data set (done by the *source_spectrum* class in module u2). In the second stage, its amplitude is adjusted in the 'estimate

average initial amplitudes' step of Figure 4, i.e. in the first iteration of the nonlinear inversion undertaken by the h13 module. The criterion used for fixing the amplitude of $P(\omega)$, is that the energies of the initially predicted data should mach those of the observed data, in some average sense. We choose to fit the decay of observed energies as a function of distance (see Figure 5).

3.5. Detailing of individual code files

3.5.1. Core ANSEICCA programs or modules: the anseicca directory

- *anseicca_wrapper_serial* or *anseicca_wrapper_parallel*: wrapper for the serial or parallel versions of the code, respectively.

- *hans2013_serial* and *hans2013_parallel*: serial and parallel versions respectively, of the 'core' code module.

- *view_output_anseicca*: module used for visualization of code output; requires a pickle file, or directory containing pickle files, as input.

3.5.2. Utility modules: the modules_common directory

- *config*: configuration module containing definitions of globally used functions and user-defined data structures; assigns values to various simulation parameters by reading the Par_file using Python's *configparser* utility.

- *cctomo_utils1*: contains the mandatorily required code utilities, i.e. those which are independent of whether the data is internal or external — set up of the modeling domain, adding Gaussian noise to synthetic cross-correlations, all types of source (model) parameterizations, inversion.

- *cctomo_utils2*: contains those code utilities which are relevant only in case of external data (see section RD above) — fitting of $1/r$ curve to cross-correlation energy as a function of distance, estimation of the source power spectrum $P(\omega)$, reading and processing of data, calculation/assignment of data errors.

- *read_pickle_output*: reads the code output, i.e. the pickle file produced by *utils_io*; also does the groundwork for some of the operations of *view_output_anseicca*.

- *utils_io*: handles all input/output operations. For input, it reads the stations file and velocity/structure model files. The input models are currently limited to 1-D (depth-dependent) elastic and 2-D (x-y?) acoustic models.

- *utils_plotting*: contains various plotting utilities.

- *validate_params*: performs basic checks on parameter values (for aliasing, memory requirement etc.), before the core code is allowed to run.

Compute time (s)						
Grid size \ Number of receivers	10		20		50	
	Serial	Parallel	Serial	Parallel	Serial	Parallel
51×51	5	6	15	13	79	55
101×101	19	11	69	16	432	75
201×201	68	34	285	99	1958	374

Table 2
Computing time to complete one iteration of inversion, for various model sizes and receiver array densities. The number of processors (cores) used is equal to the number of receivers, in each case (see main text for explanation).

4. Benchmarking

We provide some performance benchmarks using variations of the 'E1' example provided along with the package, which corresponds to the test model shown in Figure 2(a). The canonical setup for this example entails 20 receivers, a center frequency of 0.2 Hz and a model size of 101×101 grid points (see Datta et al., 2023). Here we perform inversions using essentially the same setup, but with three different model sizes and either 10, 20 or 50 receivers (Figure 6). Note that 'model size' here refers to the number of grid points, not the number of model parameters, which is the same in all tests (625, see Datta et al., 2023). These benchmark tests are run on an HPC system with 2.9 GHz Intel Xeon Platinum 8268 processors, and 48 processors per node.

For each test, the time required to complete one iteration of inversion, is listed in Table 2. These times include the time taken to generate the test data, because the code is run in internal data mode. Note how the difference between the serial and parallel compute times, scales with the number of receivers. For reference, a complete inversion in the most compute-heavy scenario, 201×201 grid and 50 receivers, took just over an hour (3800 s), with 15 iterations.

We wish to point out that the same tests run significantly faster on an iMac with a 3.6 GHz Intel Core i9 processor, and 64 GB RAM. For example with 50 receivers, the serial code on the iMac yields single-iteration run times of 57, 261 and 1070 s, for the three model sizes considered. Yet faster run times are achieved on an iMac with an Apple M1 chip. We are unable to run the parallel code on the iMacs, due to the small number of processors available (< 10).

5. Discussion and Conclusion

We have presented a useful computational seismology package, ANSEICCA, for seismic ambient noise cross-correlation modelling and noise source inversion, at local scales. It is written in Python and has been parallelised for efficiency. At a deeper level, it utilizes optimized C code for seismic wave propagation modelling in heterogeneous media, but this too is facilitated by a Python package (Devito), so the convenience of the Python environment is maintained throughout.

ANSEICCA is extremely 'lightweight' – it has no storage requirements and its memory requirements, on the order of one to tens of GB depending on grid size, are easily met by modern computers. It is also highly modular, which makes it easily extensible. For example, it currently leverages Devito for 2-D acoustic modelling. This can be augmented to 3-D elastic modelling in future, simply by writing a new module to interface with Devito. Taking this idea a step further, ANSEICCA could also be linked to other wave propagation solvers in future, should the need arise to go beyond Devito.

The lmitations of ANSEICCA, from an implementation perspective, are its rigid cartesian grid (which cannot account for Earth's sphericity or surface topography), and the approximation of integrals with weighted sums. Additionally, empirical tests reveal that the code slows down substantially when the number of model parameters (basis functions) exceeds 10^4 in order of magnitude. However, 10^4 should be sufficient for most local scale applications. This study, and all related previous works, have used less than 10^3 model parameters.

From a methodological point of view, there are currently two key limitations — the assumption of a uniform noise source spectrum, and the inability to account for the Earth's three-dimensional elastic (or anelastic) structure. Both of these are algorithmic issues, which will require modification of the forward or inverse problem solutions, without any conceptual changes to the source inversion scheme.

With these challenges in mind, we intend to continuously maintain and further develop the ANSEICCA package. This paper makes ANSEICCA accessible for immediate use as well as development by other interested researchers in the community.

6. Acknowledgements

I thank Shravan Hanasoge for providing the seed MATLAB code in 2018, for the calculation of source sensiticity kernels, which lie at the heart of this package. Thank you to Bharath Shekar for helping to interface ANSEICCA with Devito, to Pushp Lochan Kumar and Aileni Mahesh for extensive code testing and benchmarking over the last two years, and to the latter for writing the user manual accompanying the software. The support and resources provided by the Param Brahma HPC facility under the National Supercomputing Mission, Government of India, at IISER Pune are gratefully acknowledged.

7. Code availability

The ANSEICCA package is available at `https://github.com/arjundatta23/cc_kern_inv`. Supporting code is available at `https://github.com/arjundatta23/SW1D_earthsr` (for *SW1D_earthsr*) and `https://github.com/devitocodes/devito` (for *Devito*).

References

Aso, N., Tsai, V.C., Schoof, C., Flowers, G.E., Whiteford, A., Rada, C., 2017. Seismologically observed spatiotemporal drainage activity at moulins. Journal of Geophysical Research: Solid Earth 122, 9095–9108. URL: https://onlinelibrary.wiley.com/doi/full/10.1002/2017JB014578https://onlinelibrary.wiley.com/doi/abs/10.1002/2017JB014578https://agupubs.onlinelibrary.wiley.com/doi/10.1002/2017JB014578, doi:10.1002/2017JB014578.

Bensen, G.D., Ritzwoller, M.H., Barmin, M.P., Levshin, A.L., Lin, F., Moschetti, M.P., Shapiro, N.M., Yang, Y., 2007. Processing seismic ambient noise data to obtain reliable broad-band surface wave dispersion measurements. Geophysical Journal International 169, 1239–1260. URL: https://academic.oup.com/gji/article-lookup/doi/10.1111/j.1365-246X.2007.03374.x, doi:10.1111/j.1365-246X.2007.03374.x.

Bowden, D.C., Tsai, V.C., Lin, F.C., 2015. Site amplification, attenuation, and scattering from noise correlation amplitudes across a dense array in long beach, ca. Geophysical Research Letters doi:10.1002/2014GL062662.

Cros, E., Roux, P., Vandemeulebrouck, J., Kedar, S., 2011. Locating hydrothermal acoustic sources at old faithful geyser using matched field processing. Geophysical Journal International 187, 385–393. URL: https://academic.oup.com/gji/article/187/1/385/562800, doi:10.1111/J.1365-246X.2011.05147.X/3/187-1-385-FIG009.JPEG.

Dalcín, L., Paz, R., Storti, M., 2005. MPI for Python. J. Parallel Distrib. Comput. 65, 1108 – 1115. doi:10.1016/j.jpdc.2005.03.010.

Datta, A., 2018. Swrt: A package for semi-analytical solutions of surface wave propagation, including mode conversion, across transversely aligned vertical discontinuities. Geoscientific Instrumentation, Methods and Data Systems 7, 101–112. URL: https://www.geosci-instrum-method-data-syst.net/7/101/2018/, doi:10.5194/gi-7-101-2018.

Datta, A., 2023. Reply to comment on Malkoti et al. (2021) by Haney and Nakahara. Geophysical Journal International 234, 1965–1969. URL: https://academic.oup.com/gji/article/234/3/1965/7146201, doi:10.1093/GJI/GGAD179.

Datta, A., Hanasoge, S., Goudswaard, J., 2019. Finite frequency inversion of cross-correlation amplitudes for ambient noise source directivity estimation. Journal of Geophysical Research: Solid Earth 124, 6653–6665. URL: https://onlinelibrary.wiley.com/doi/abs/10.1029/2019JB017602, doi:10.1029/2019JB017602.

Datta, A., Priestley, K.F., Roecker, S., Chapman, C.H., 2017. Surface wave mode coupling and the validity of the path average approximations in surface waveform inversions: an empirical assessment. Geophys. J. Int. 211, 1099–1120.

Datta, A., Shekar, B., Kumar, P.L., 2023. Acoustic full waveform inversion for 2-d ambient noise source imaging. Geophysical Journal International 234, 1628–1639. URL: https://academic.oup.com/gji/article/234/3/1628/7117958, doi:10.1093/GJI/GGAD158.

Delaney, E., Ermert, L., Sager, K., Kritski, A., Bussat, S., Fichtner, A., 2017. Passive seismic monitoring with nonstationary noise sources. GEOPHYSICS 82, KS57–KS70. URL: http://library.seg.org/doi/10.1190/geo2016-0330.1, doi:10.1190/geo2016-0330.1.

Denolle, M.A., Dunham, E.M., Prieto, G.A., Beroza, G.C., 2013. Ground motion prediction of realistic earthquake sources using the ambient seismic field. Journal of Geophysical Research: Solid Earth 118, 2102–2118. doi:10.1029/2012JB009603.

Ermert, L., Igel, J., Sager, K., Stutzmann, E., Nissen-Meyer, T., Fichtner, A., 2020. Introducing noisi: A python tool for ambient noise cross-correlation modeling and noise source inversion. Solid Earth 11, 1597–1615. doi:10.5194/SE-11-1597-2020.

Ermert, L., Sager, K., Afanasiev, M., Boehm, C., Fichtner, A., 2017. Ambient seismic source inversion in a heterogeneous earth: Theory and application to the earth's hum. Journal of Geophysical Research: Solid Earth 122, 9184–9207. URL: http://doi.wiley.com/10.1002/2017JB014738, doi:10.1002/2017JB014738.

Ermert, L., Villaseñor, A., Fichtner, A., 2016. Cross-correlation imaging of ambient noise sources. Geophysical Journal International 204, 347–364. URL: https://academic.oup.com/gji/article-lookup/doi/10.1093/gji/ggv460, doi:10.1093/gji/ggv460.

Fichtner, A., 2014. Source and processing effects on noise correlations. Geophysical Journal International 197, 1527–1531. URL: http://academic.oup.com/gji/article/197/3/1527/657661/Source-and-processing-effects-on-noise, doi:10.1093/gji/ggu093.

Fichtner, A., Stehly, L., Ermert, L., Boehm, C., 2017. Generalized interferometry – i: theory for interstation correlations. Geophysical Journal International 208, 603–638. URL: https://academic.oup.com/gji/article-lookup/doi/10.1093/gji/ggw420, doi:10.1093/gji/ggw420.

Fichtner, A., Tsai, V.C., 2019. Theoretical Foundations of Noise Interferometry, in: Nakata, N., Gualtieri, L., Fichtner, A. (Eds.), Seismic Ambient Noise. 1 ed.. Cambridge University Press, pp. 109–143. URL: https://www.cambridge.org/core/product/identifier/9781108264808%23c4/type/book_part, doi:10.1017/9781108264808.006.

Froment, B., Campillo, M., Roux, P., Gouédard, P., Verdel, A., Weaver, R.L., 2010. Estimation of the effect of nonisotropically distributed energy on the apparent arrival time in correlations. GEOPHYSICS 75, SA85–SA93. URL: http://library.seg.org/doi/10.1190/1.3483102, doi:10.1190/1.3483102.

Gomberg, J.S., Masters, T.G., 1988. Waveform modelling using locked-mode synthetic and differential seismograms: application to determination of the structure of mexico. Geophysical Journal 94, 193–218. doi:10.1111/j.1365-246X.1988.tb05896.x.

Halliday, D., Curtis, A., 2008. Seismic interferometry, surface waves and source distribution. Geophysical Journal International 175, 1067–1087. URL: https://academic.oup.com/gji/article-lookup/doi/10.1111/j.1365-246X.2008.03918.x, doi:10.1111/j.1365-246X.2008.03918.x.

Hanasoge, S.M., 2013. The influence of noise sources on cross-correlation amplitudes. Geophysical Journal International 192, 295–309. URL: http://academic.oup.com/gji/article/192/1/295/594723/The-influence-of-noise-sources-on-crosscorrelation, doi:10.1093/gji/ggs015.

Hanasoge, S.M., 2014. Measurements and kernels for source-structure inversions in noise tomography. Geophysical Journal International 196, 971–985. doi:10.1093/gji/ggt411.

Igel, J.K., Bowden, D.C., Fichtner, A., 2023. Sans: Publicly available daily multi-scale seismic ambient noise source maps. Journal of Geophysical Research: Solid Earth 128, e2022JB025114. URL: https://onlinelibrary.wiley.com/doi/full/10.1029/2022JB025114https://onlinelibrary.wiley.com/doi/abs/10.1029/2022JB025114https://agupubs.onlinelibrary.wiley.com/doi/10.1029/2022JB025114, doi:10.1029/2022JB025114.

Igel, J.K., Ermert, L.A., Fichtner, A., 2021. Rapid finite-frequency microseismic noise source inversion at regional to global scales. Geophysical Journal International 227, 169–183. URL: https://academic.oup.com/gji/article/227/1/169/6287575, doi:10.1093/GJI/GGAB210.

Juretzek, C., Hadziioannou, C., 2016. Where do ocean microseisms come from? a study of love-to-rayleigh wave ratios. Journal of Geophysical Research: Solid Earth 121, 6741–6756. URL: https://onlinelibrary.wiley.com/doi/full/10.1002/2016JB013017https://onlinelibrary.wiley.com/doi/abs/10.1002/2016JB013017https://agupubs.onlinelibrary.wiley.com/doi/10.1002/2016JB013017, doi:10.1002/2016JB013017.

Kimman, W.P., Trampert, J., 2010. Approximations in seismic interferometry and their effects on surface waves. Geophysical Journal International 182, 461–476. URL: https://academic.oup.com/gji/article-lookup/doi/10.1111/j.1365-246X.2010.04632.x, doi:10.1111/j.1365-246X.2010.04632.x.

Labedz, C.R., Bartholomaus, T.C., Amundson, J.M., Gimbert, F., Karplus, M.S., Tsai, V.C., Veitch, S.A., 2022. Seismic mapping of subglacial hydrology reveals previously undetected pressurization event. Journal of Geophysical Research: Earth Surface , e2021JF006406URL: https://onlinelibrary.wiley.com/doi/full/10.1029/2021JF006406https://onlinelibrary.wiley.com/doi/abs/10.1029/2021JF006406https://agupubs.onlinelibrary.wiley.com/doi/10.1029/2021JF006406, doi:10.1029/

2021JF006406.

Lehujeur, M., Vergne, J., Maggi, A., Schmittbuhl, J., 2017. Ambient noise tomography with non-uniform noise sources and low aperture networks: case study of deep geothermal reservoirs in northern alsace, france. Geophysical Journal International 208, 193–210. URL: https://academic.oup.com/gji/article-lookup/doi/10.1093/gji/ggw373, doi:10.1093/gji/ggw373. they have produced rose-diagram figures (see Fig 10) similar to the ones from my azimuthal analysis.

Lobkis, O.I., Weaver, R.L., 2001. On the emergence of the green's function in the correlations of a diffuse field. The Journal of the Acoustical Society of America 110, 3011–3017. URL: http://asa.scitation.org/doi/10.1121/1.1417528, doi:10.1121/1.1417528.

Louboutin, M., Lange, M., Luporini, F., Kukreja, N., Witte, P.A., Herrmann, F.J., Velesko, P., Gorman, G.J., 2019. Devito (v3.1.0): an embedded domain-specific language for finite differences and geophysical exploration. Geoscientific Model Development 12, 1165–1187. URL: https://www.geosci-model-dev.net/12/1165/2019/, doi:10.5194/gmd-12-1165-2019.

Luporini, F., Louboutin, M., Lange, M., Kukreja, N., Witte, P., Hückelheim, J., Yount, C., Kelly, P.H.J., Herrmann, F.J., Gorman, G.J., 2020. Architecture and performance of devito, a system for automated stencil computation. ACM Trans. Math. Softw. 46. URL: https://doi.org/10.1145/3374916, doi:10.1145/3374916.

Malkoti, A., Datta, A., Hanasoge, S.M., 2021. Rayleigh-wave h/v ratio measurement from ambient noise cross-correlations and its sensitivity to vp: a numerical study. Geophysical Journal International 227, 472–482. URL: https://academic.oup.com/gji/article/227/1/472/6296642, doi:10.1093/GJI/GGAB228.

Menke, W., 2012. Geophysical Data Analysis: Discrete Inverse Theory. Academic Press.

Pedersen, H.A., Krüger, F., 2007. Influence of the seismic noise characteristics on noise correlations in the baltic shield. Geophysical Journal International 168, 197–210. URL: https://academic.oup.com/gji/article-lookup/doi/10.1111/j.1365-246X.2006.03177.x, doi:10.1111/j.1365-246X.2006.03177.x.

Retailleau, L., Gualtieri, L., 2019. Toward high-resolution period-dependent seismic monitoring of tropical cyclones. Geophysical Research Letters 46, 1329–1337. URL: https://onlinelibrary.wiley.com/doi/full/10.1029/2018GL080785https://onlinelibrary.wiley.com/doi/abs/10.1029/2018GL080785https://agupubs.onlinelibrary.wiley.com/doi/10.1029/2018GL080785, doi:10.1029/2018GL080785.

Roten, D., Fäh, D., Cornou, C., Giardini, D., 2006. Two-dimensional resonances in alpine valleys identified from ambient vibration wavefields. Geophysical Journal International 165, 889–905. doi:10.1111/J.1365-246X.2006.02935.X/3/165-3-889-FIG031.JPEG.

Roux, P., 2009. Passive seismic imaging with directive ambient noise: application to surface waves and the san andreas fault in parkfield, ca. Geophysical Journal International 179, 367–373. URL: https://academic.oup.com/gji/article-lookup/doi/10.1111/j.1365-246X.2009.04282.x, doi:10.1111/j.1365-246X.2009.04282.x.

Sager, K., Boehm, C., Ermert, L., Krischer, L., Fichtner, A., 2018a. Sensitivity of seismic noise correlation functions to global noise sources. Journal of Geophysical Research: Solid Earth URL: http://doi.wiley.com/10.1029/2018JB016042, doi:10.1029/2018JB016042.

Sager, K., Ermert, L., Boehm, C., Fichtner, A., 2018b. Towards full waveform ambient noise inversion. Geophysical Journal International 212, 566–590. URL: http://academic.oup.com/gji/article/212/1/566/4411809, doi:10.1093/gji/ggx429.

Shapiro, N.M., Campillo, M., 2004. Emergence of broadband rayleigh waves from correlations of the ambient seismic noise. Geophysical Research Letters 31, n/a–n/a. URL: http://doi.wiley.com/10.1029/2004GL019491, doi:10.1029/2004GL019491.

Snieder, R., 2004. Extracting the green's function from the correlation of coda waves: A derivation based on stationary phase. Physical Review E 69, 046610. URL: https://journals.aps.org/pre/abstract/10.1103/PhysRevE.69.046610, doi:10.1103/PhysRevE.69.046610.

Stehly, L., Boué, P., 2017. On the interpretation of the amplitude decay of noise correlations computed along a line of receivers. Geophysical Journal

International 209, 358–372. URL: https://academic.oup.com/gji/article-lookup/doi/10.1093/gji/ggx021, doi:10.1093/gji/ggx021.

Tarantola, A., 2005. Inverse Problem Theory and Methods for Model Parameter Estimation. Society for Industrial and Applied Mathematics. doi:10.1137/1.9780898717921.

Tkalčić, H., Pham, T.S., Wang, S., 2020. The earth's coda correlation wavefield: Rise of the new paradigm and recent advances. Earth-Science Reviews 208, 103285. doi:10.1016/J.EARSCIREV.2020.103285.

Tromp, J., Dahlen, F.A., 1993. Variational principles for surface wave propagation on a laterally heterogeneous earth—iii. potential representation. Geophysical Journal International 112, 195–209. URL: https://dx.doi.org/10.1111/j.1365-246X.1993.tb01449.x, doi:10.1111/J.1365-246X.1993.TB01449.X.

Tromp, J., Luo, Y., Hanasoge, S., Peter, D., 2010. Noise cross-correlation sensitivity kernels. Geophysical Journal International 183, 791–819. URL: https://academic.oup.com/gji/article-lookup/doi/10.1111/j.1365-246X.2010.04721.x, doi:10.1111/j.1365-246X.2010.04721.x.

Tsai, V.C., 2009. On establishing the accuracy of noise tomography travel-time measurements in a realistic medium. Geophysical Journal International 178, 1555–1564. URL: https://academic.oup.com/gji/article-lookup/doi/10.1111/j.1365-246X.2009.04239.x, doi:10.1111/j.1365-246X.2009.04239.x.

Tsai, V.C., 2011. Understanding the amplitudes of noise correlation measurements. Journal of Geophysical Research 116, B09311. URL: http://doi.wiley.com/10.1029/2011JB008483, doi:10.1029/2011JB008483.

Tsai, V.C., Minchew, B., Lamb, M.P., Ampuero, J.P., 2012. A physical model for seismic noise generation from sediment transport in rivers. Geophysical Research Letters 39, 2404. URL: https://onlinelibrary.wiley.com/doi/full/10.1029/2011GL050255https://onlinelibrary.wiley.com/doi/abs/10.1029/2011GL050255https://agupubs.onlinelibrary.wiley.com/doi/10.1029/2011GL050255, doi:10.1029/2011GL050255.

Wang, K., Luo, Y., Yang, Y., 2016. Correction of phase velocity bias caused by strong directional noise sources in high-frequency ambient noise tomography: a case study in karamay, china. Geophysical Journal International 205, 715–727. URL: https://academic.oup.com/gji/article-lookup/doi/10.1093/gji/ggw039, doi:10.1093/gji/ggw039.

Wapenaar, K., 2004. Retrieving the elastodynamic green's function of an arbitrary inhomogeneous medium by cross correlation. Physical Review Letters 93, 254301. URL: https://link.aps.org/doi/10.1103/PhysRevLett.93.254301, doi:10.1103/PhysRevLett.93.254301.

Wapenaar, K., Draganov, D., Snieder, R., Campman, X., Verdel, A., 2010. Tutorial on seismic interferometry: Part 1 — basic principles and applications. https://doi.org/10.1190/1.3457445 75. URL: https://library.seg.org/doi/10.1190/1.3457445, doi:10.1190/1.3457445.

Xu, Z., Mikesell, T.D., Gribler, G., Mordret, A., 2019. Rayleigh-wave multicomponent cross-correlation-based source strength distribution inversion. part 1: Theory and numerical examples. Geophysical Journal International 218, 1761–1780. URL: https://academic.oup.com/gji/article/218/3/1761/5510447, doi:10.1093/gji/ggz261.

Yao, H., van der Hilst, R.D., 2009. Analysis of ambient noise energy distribution and phase velocity bias in ambient noise tomography, with application to se tibet. Geophysical Journal International 179, 1113–1132. URL: https://academic.oup.com/gji/article-lookup/doi/10.1111/j.1365-246X.2009.04329.x, doi:10.1111/j.1365-246X.2009.04329.x.

8. APPENDIX 1: Inversion algorithm

Equation (5) can be written as

$$\chi = \frac{1}{2}\sum_i \Delta d_i^2, \tag{10}$$

where $\Delta d_i = \ln E_i^{\mathrm{obs}} - \ln E_i^{\mathrm{syn}}$.

Variations in the misfit are related to variations in the model parameters (spatial source distribution $\sigma(\mathbf{x})$) via the misfit kernel $K(\mathbf{x})$:

$$\delta\chi = -\int K(\mathbf{x})\delta\sigma(\mathbf{x})\,\mathrm{d}^2\mathbf{x} \tag{11}$$

Since the model space is parameterized using a set of 2-D Gaussian basis functions (Datta et al., 2023):

$$\sigma(\mathbf{x}) = \sum_j m_j^2 B_j(\mathbf{x}), \tag{12}$$

the model perturbation can be expanded into the model space basis functions, $B_j(\mathbf{x})$:

$$\delta\sigma(\mathbf{x}) = \sum_{j=1}^{M} 2m_j\delta m_j B_j(\mathbf{x}) \tag{13}$$

Also, the misfit kernel is the sum of individual source kernels for each receiver pair, weighted by the corresponding data misfit:

$$K = \sum_i \Delta d_i K_i(\mathbf{x}) = \sum_i \ln\left(\frac{E_i^{\mathrm{obs}}}{E_i^{\mathrm{syn}}}\right) K_i(\mathbf{x}) \tag{14}$$

As shown in Datta et al. (2019, 2023), equations (11), (13) and (14) produce the gradient $\mathbf{g}$ of χ, as well as the Jacobian matrix ($\mathbf{G}$) which linearizes the inverse problem:

$$g_j = \frac{\partial\chi}{\partial m_j} = -\int 2K(\mathbf{x})m_j B_j(\mathbf{x})\,\mathrm{d}^2\mathbf{x} = -G_{ij}\Delta d_i, \tag{15}$$

where

$$G_{ij} = \int 2K_i(\mathbf{x})m_j B_j(\mathbf{x})\mathrm{d}^2\mathbf{x}. \tag{16}$$

In matrix notation, we have

$$\mathbf{g} = -\mathbf{G}^T \Delta\mathbf{d} \tag{17}$$

Similarly, the Jacobian matrix yields the approximate Hessian for a Gauss-Newton inversion:

$$\mathbf{H} = \mathbf{G}^T \mathbf{G} \tag{18}$$

In practice, equations (17) and (18) are modified to incorporate weighting and damping (see e.g. Menke, 2012):

$$\begin{aligned} \tilde{\mathbf{g}} &= -\mathbf{G}^T \mathbf{C}_D^{-1} \Delta\mathbf{d} - \mathbf{C}_M^{-1} \left(\mathbf{m} - \mathbf{m}_0\right) \\ \tilde{\mathbf{H}} &= \mathbf{G}^T \mathbf{C}_D^{-1} \mathbf{G} + \mathbf{C}_M^{-1} \end{aligned} \tag{19}$$

where $\mathbf{C}_D$ and $\mathbf{C}_M$ are the data and model covariance matrices, respectively, and $\mathbf{m}_0$ is a prior model about which the inversion is damped (also serving as the starting model for iterative inversion). The form of damping represented by equation (19) requires that the the model vector comprises the basis function coefficients, m_j. Hence it is these coefficients that are directly updated by iterative optimization. The Gauss-Newton method (Menke, 2012; Tarantola, 2005) yields:

$$\left[\mathbf{G}_k^T \mathbf{C}_D^{-1} \mathbf{G}_k + \mathbf{C}_M^{-1}\right] \Delta\mathbf{m}_k = \left[\mathbf{G}_k^T \mathbf{C}_D^{-1} \Delta\mathbf{d}_k + \mathbf{C}_M^{-1} \left(\mathbf{m}_k - \mathbf{m}_0\right)\right] \tag{20}$$

or

$$\mathbf{m}_{k+1} = \mathbf{m}_k + \left[\mathbf{G}_k^T \mathbf{C}_D^{-1} \mathbf{G}_k + \mathbf{C}_M^{-1}\right]^{-1} \left[\mathbf{G}_k^T \mathbf{C}_D^{-1} \Delta\mathbf{d}_k + \mathbf{C}_M^{-1} \left(\mathbf{m}_k - \mathbf{m}_0\right)\right] \tag{21}$$

We note that this is mathematically equivalent (see Tarantola, 2005) to the expression

$$\mathbf{m}_{k+1} = \mathbf{m}_0 + \mathbf{C}_M \mathbf{G}_k^T \left[\mathbf{G}_k \mathbf{C}_M \mathbf{G}_k^T + \mathbf{C}_D\right]^{-1} \left[\Delta\mathbf{d}_k + \mathbf{G}_k \left(\mathbf{m}_k - \mathbf{m}_0\right)\right] \tag{22}$$

List of Figures

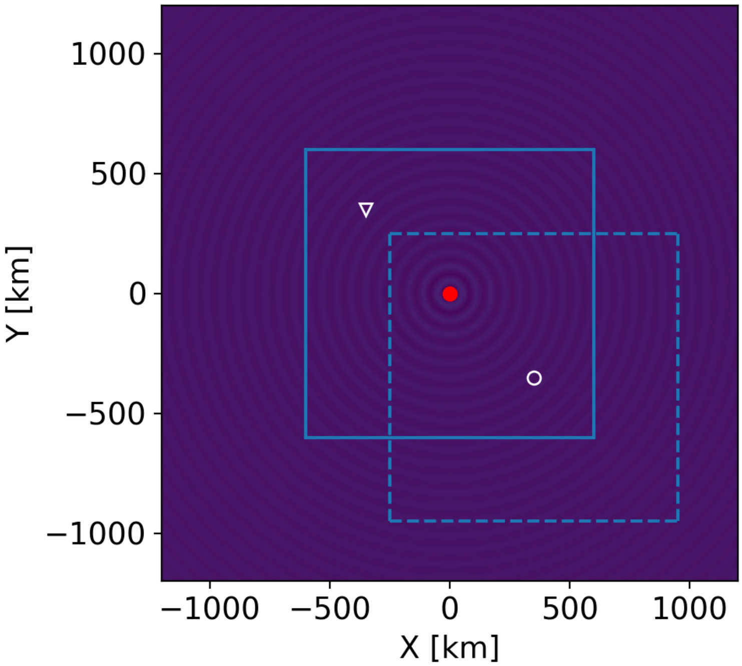

Figure 1: 'Outer domain' source trick used for laterally homogeneous media, illustrated using the modelling geometry of Malkoti et al. (2021). Here the actual modelling domain is of size 1200×1200 km, shown by the inner square with solid lines. The desired quantity is the Green's function throughout this domain, due to a source at the receiver location marked by the inverted triangle. In the ANSEICCA implementation, an outer domain of size 2400×2400 km is used and the Green's function calculated throughout it, for a source at the origin (red dot). The obtained solution is shown here in colour, at some arbitrary frequency. The desired quantity is then obtained by simply windowing this outer domain solution, using the square marked with dashed lines. This square is the same size as the actual domain, but is centred (open white circle) at the mirror image, with respect to the origin, of the actual receiver location. Thus by positioning the window appropriately, the solution can be obtained for a source at any location within the modelling domain.

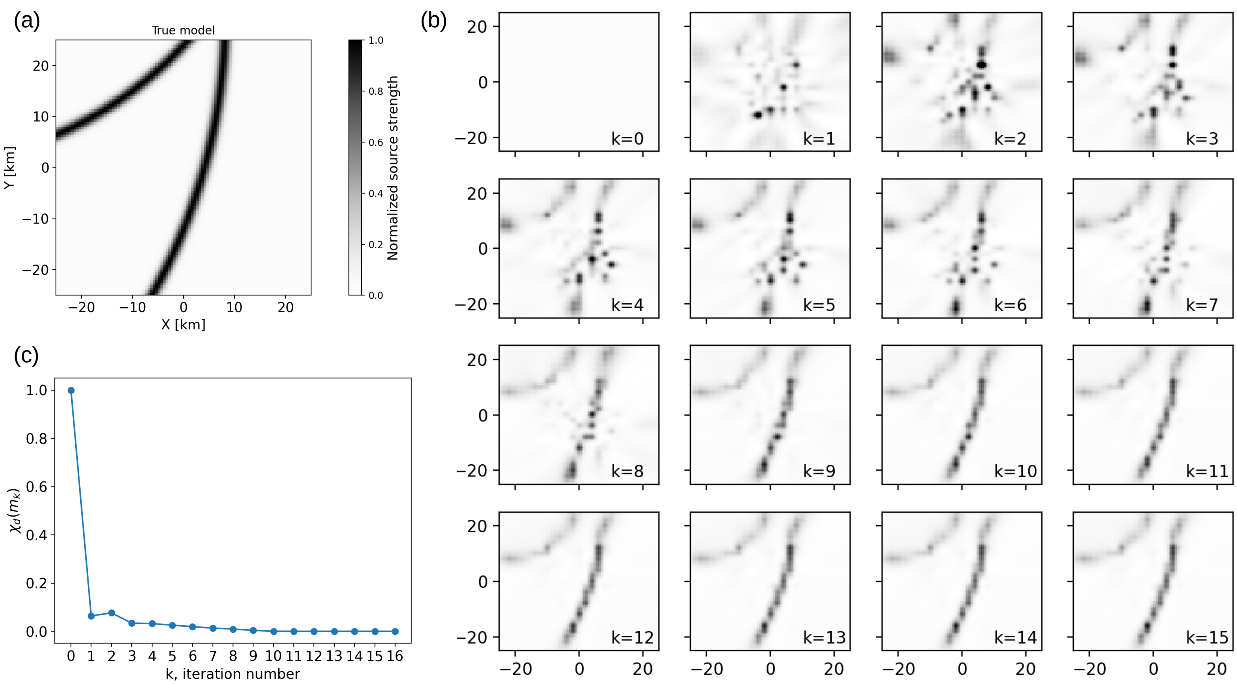

Figure 2: Synthetic test to illustrate inversion progress. (a) The test model for the E1 example; note that this is the same model as in Figure 2d of Datta et al. (2023). (b) Evolution of the model with progress of inversion (as indicated by the iteration number k in each panel); note the homogeneous starting model in the top left, and the inversion result in the bottom right. (c) Evolution of data misfit, showing $\approx 99\%$ misfit reduction in this synthetic example.

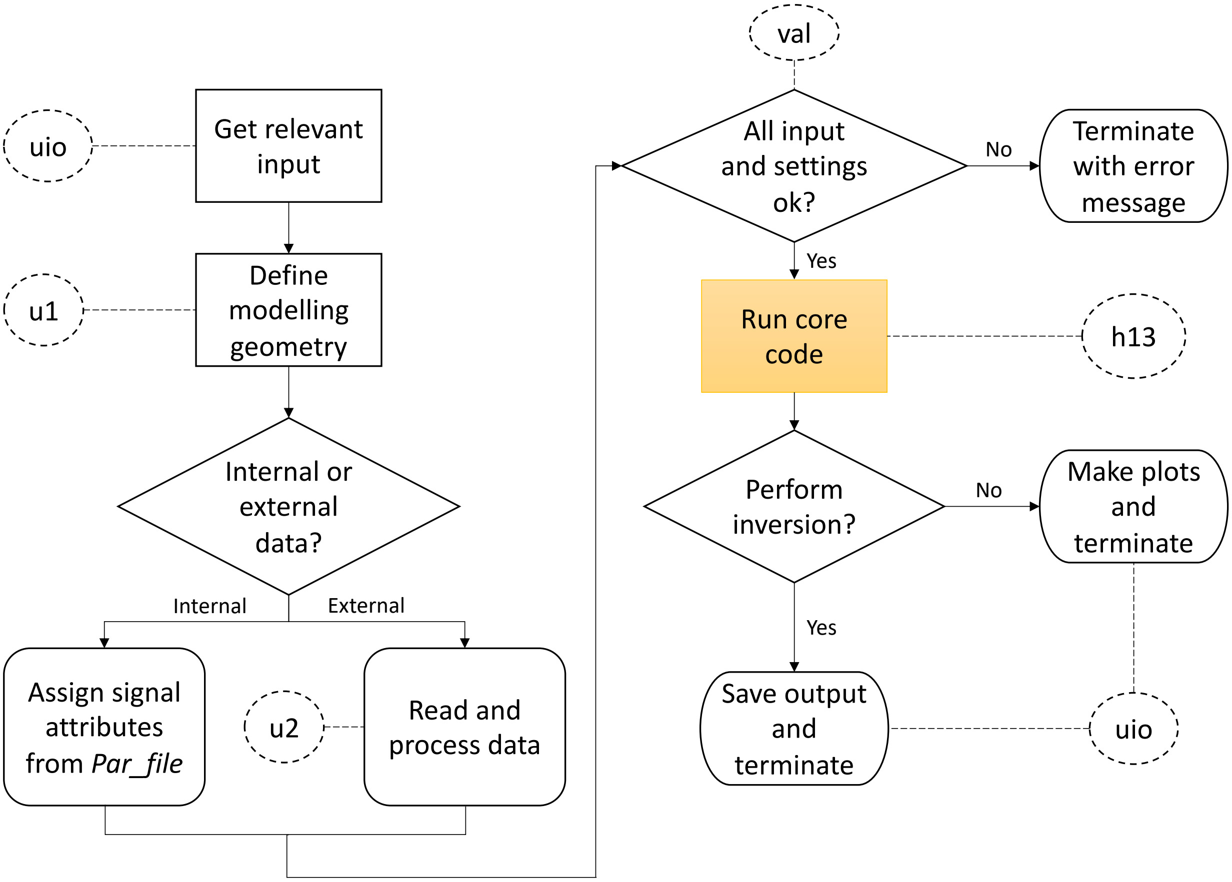

Figure 3: Flowchart of the overall structure of the package, essentially mirroring the wrapper programs. The highlighted (yellow) process in this flowchart is the one that is parallelised (see Section 3.3). The dashed circular inputs associated with any step or process represent the modules used for its implementation, as per the nomenclature of Table 1. We note that the *config* module is not shown here, but is used ubiquitously. See Section 3.2.1 for the definitions of 'internal/external' data.

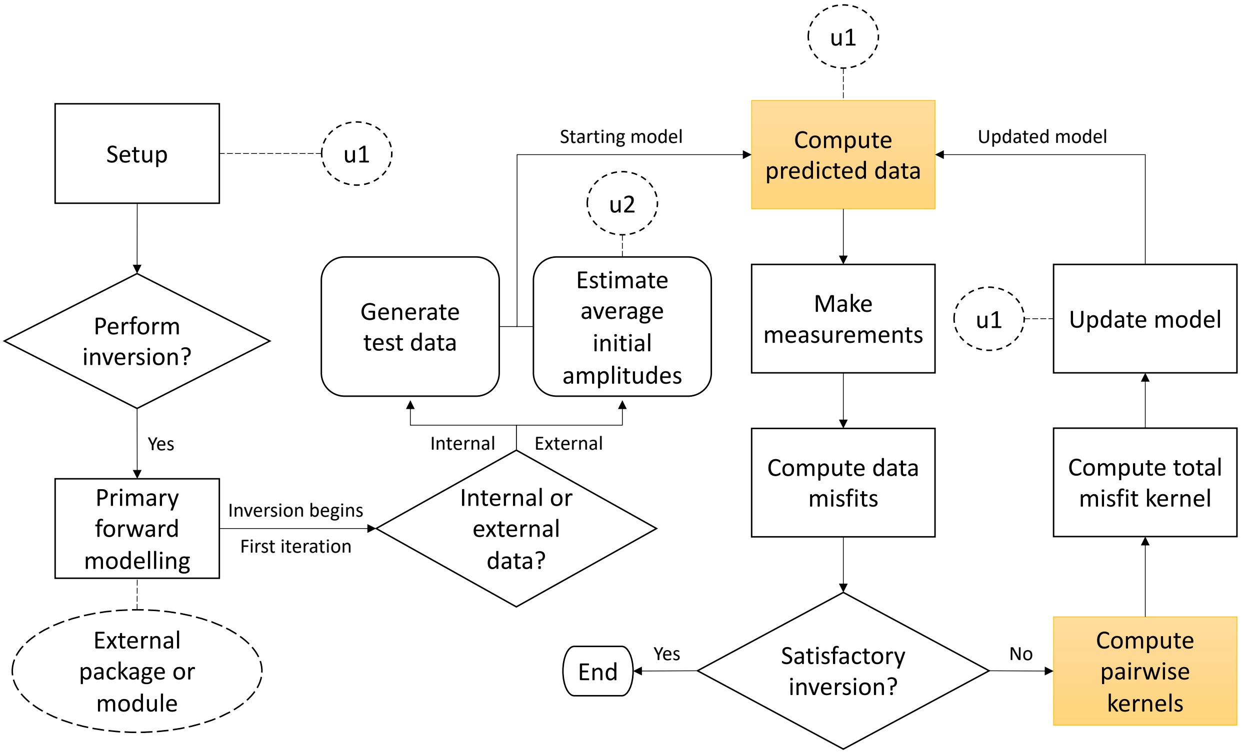

Figure 4: Flowchart showing the detailed structure of the core module, h13. The two highlighted boxes, which are part of the inversion loop, represent code operations that are parallelized. Other symbols have the same meaning as in Figure 3.

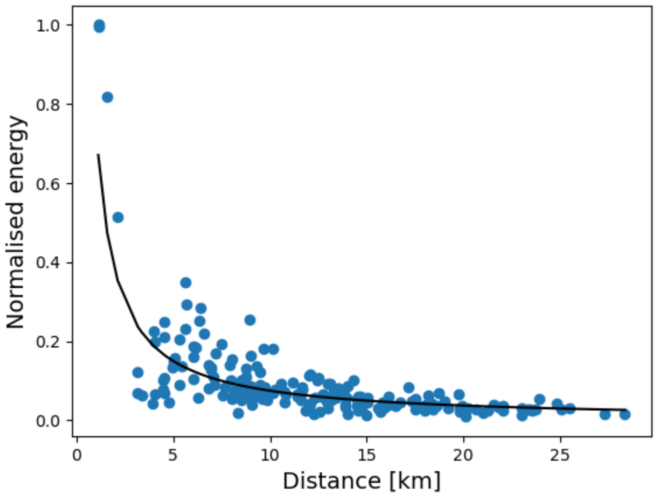

Figure 5: Example of curve-fitting for observed cross-correlation energy as a function of inter-receiver distance r, taken from the test data of example E1. The blue circles show the observed energies, and the black line is the best fitting $1/r$ curve. Energies are normalised with respect to the maximum observed value. First-iteration synthetics in an inversion will be scaled such that their energies match the black curve.

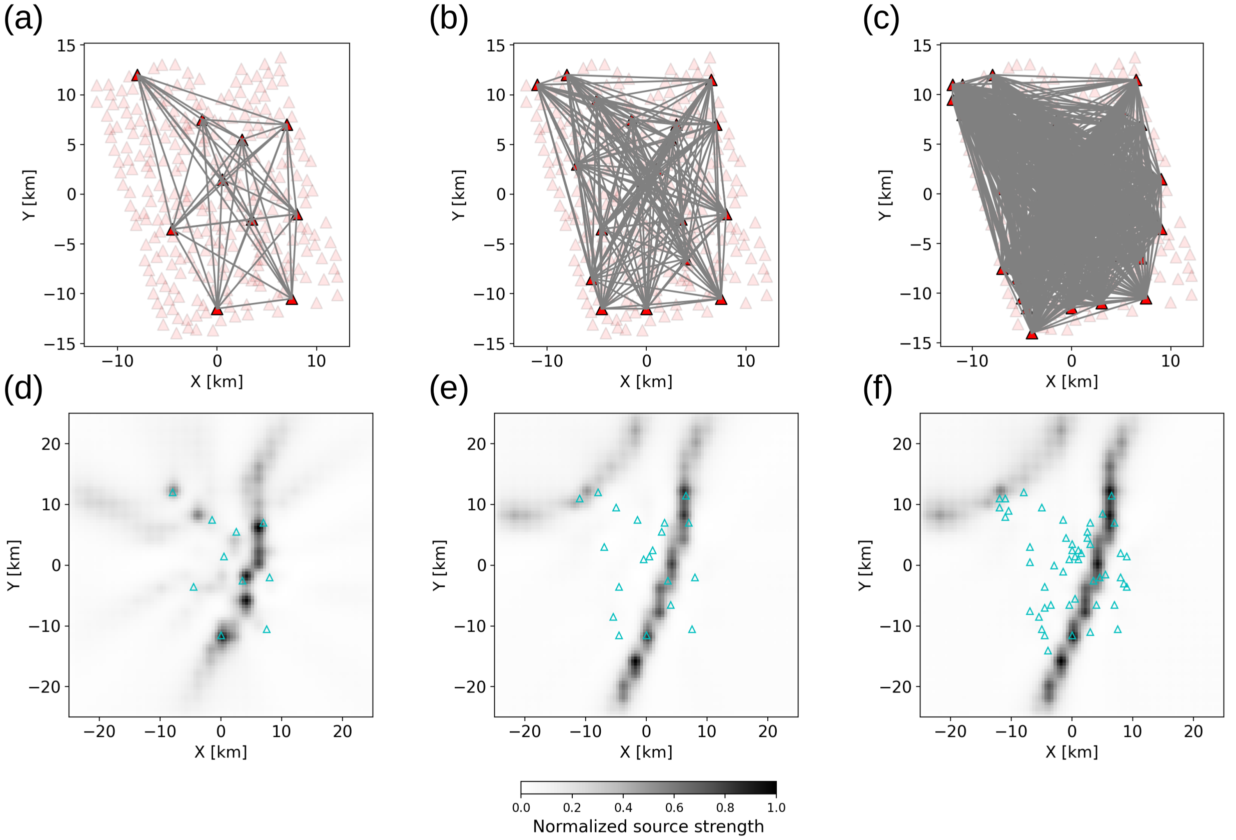

Figure 6: Inversion setup and results related to the benchmark tests. (a)-(c) Receiver maps showing the selection of 10, 20 and 50 receivers (dark red triangles), along with inter-receiver paths (grey lines). (d)-(f) Corresponding inversion results (after completion of all iterations) for a model size of 101×101. Note that (b), (e), with 20 receivers, correspond to Figure 2, where the complete inversion progress has been shown.